The Astrophysical Journal, 621:32–40, 2005 March 1
© 2005. The American Astronomical Society. All rights reserved. Printed in U.S.A.

MODELING THE EVOLUTION OF INFRARED LUMINOUS GALAXIES: THE INFLUENCE OF THE LUMINOSITY-TEMPERATURE DISTRIBUTION

G. F. Lewis,[1] S. C. Chapman,[2] and G. Helou[2]

Received 2004 May 25; accepted 2004 November 2

ABSTRACT

The evolution of the luminous infrared galaxy population is explored using a pure luminosity evolution model that incorporates the locally observed luminosity-temperature distribution for *IRAS* galaxies. Pure luminosity evolution models in a fixed ΛCDM cosmology are fitted to submillimeter and infrared counts and backgrounds. We find that the differences between the locally determined bivariate model and the single-variable luminosity function (LF) do not manifest themselves in the observed counts but rather are primarily apparent in the dust temperatures of sources in flux-limited surveys. Statistically significant differences in the redshift distributions are also observed. The bivariate model is used to predict the counts, redshifts, and temperature distributions of galaxies detectable by the *Spitzer Space Telescope*. The best-fitting model is compared to the high-redshift submillimeter galaxy population, revealing a median redshift for the total submillimeter population of $z = 1.8^{+0.9}_{-0.4}$, in good agreement with recent spectroscopic studies of submillimeter galaxies. The temperature distribution for the submillimeter galaxies is modeled to predict the radio/submillimeter indices of the submillimeter galaxies, revealing that submillimeter galaxies exhibit a broader spread in spectral energy distributions than seen in the local *IRAS* galaxies.

Subject headings: cosmology: observations — galaxies: evolution — galaxies: formation — galaxies: starburst — infrared: galaxies

Online material: color figure

1. INTRODUCTION

With an energy comparable to the optical/UV background, measurements of the far-infrared background reveal it to peak at around 200 μm (Puget et al. 1996; Fixsen et al. 1998), arising from dust reprocessing of high-energy radiation, star formation, and active galactic nucleus (AGN) activity in $z > 0$ galaxies. Such obscuration could be hiding approximately half of the massive star formation activity over the history of the universe (e.g., Blain et al. 1999a). Clearly, to unravel the cosmic history of star formation, the evolution of the infrared galaxy population needs to understood.

Studies of the evolving infrared galaxy populations have typically assumed a small range of template galaxy spectral energy distributions (SEDs) or even a single SED. However, infrared galaxies span a large range in properties, with $60/100$ μm colors spanning $\sim$0.4 dex for a given luminosity (Soifer & Neugebauer 1991; Chapman et al. 2003b). This distribution in dust SEDs implies that substantial numbers of both extremely luminous yet cold galaxies as well as low-luminosity, hot galaxies are found.

In a previous paper (Chapman et al. 2003b, hereafter C03), an evolving distribution bivariate in luminosity and color, $\Phi(L, C)$, was presented, providing consistency with the broad distribution of submillimeter galaxies observed locally. This earlier paper demonstrated that flux-limited surveys in various infrared and submillimeter bands would subsume a nonnegligible fraction of both cold, luminous galaxies and hot, faint galaxies, the predictions borne out in observations of low- and moderate-redshift *IRAS* galaxies, as well as microjansky radio sources. The overall conclusion of this study was that surveys that select objects at either the cold Raleigh-Jeans tail of the dust SED or at the hot Wien tail will preferentially detect appropriately cold or hot objects for a given luminosity class, in much larger numbers than expected if the temperature distributions were not taken into account.

Submillimeter-luminous, extragalactic sources (Smail et al. 1997) currently provide our only means of studying the high-redshift infrared galaxy population (Chapman et al. 2003c). These galaxies are now routinely detected with the JCMT/SCUBA and IRAM/MAMBO instruments, and over 200 blank-field sources are now cataloged from cluster-lensed surveys (see Blain et al. [2002] for a summary). The tight correlation observed locally between thermal far-infrared (FIR) emission and synchrotron radio emission (Helou et al. 1985; Condon 1992) allows the identification of submillimeter sources, recovering $\sim$65% of the blank-field counts (Ivison et al. 2002; Chapman et al. 2003b). With spectroscopic redshifts for the submillimeter galaxies (SMGs), the possibility exists to assess more subtle effects in our model and to understand whether our model can explain the range in properties subsumed by the SMGs, as well as to explore the implication of various selection approaches employed in submillimeter surveys.

In this paper, the bivariate model is examined in light of the multiwavelength counts and backgrounds, using a parameterization of pure luminosity evolution. The model is first used to explore predictions for the *Spitzer Space Telescope* galaxy populations in terms of their redshift, color, and temperature distributions. The model is then employed to better understand the range in properties and redshift distributions sampled by the radio-identified submillimeter galaxy population and the importance of the luminosity–dust temperature distribution, L–T and, by extrapolation, the properties of the entire submillimeter population. All calculations are undertaken in a $\Omega_0 = 0.3$, $\Lambda_0 = 0.7$, and $h = 0.65$ cosmology.

[1] Institute of Astronomy, University of Sydney, Sydney, NSW 2006, Australia; gfl@physics.usyd.edu.au.

[2] California Institute of Technology, MS 320-47, Pasadena, CA 91125; schapman@irastro.caltech.edu, ghelou@irastro.caltech.edu.

2. EVOLUTION OF THE BIVARIATE LUMINOSITY FUNCTION

The evolutionary model is anchored to the local FIR luminosity function (LF), constructed from the 1.2 Jy sample of *IRAS* galaxies (Fisher et al. 1995; C03). Recent work has emphasized the variation in dust temperature found in ultraluminous infrared galaxies (ULIRGs) with T_d as low as 25 K (Chapman et al. 2003a). The adopted form of the LF represents the distribution in dust temperatures found in the 1.2 Jy sample, parametrized by the $60/100$ μm color (a full characterization of this LF can be found in C03).

The local bivariate LF is then evolved using pure luminosity evolution with redshift. While a range of functional forms have been employed in the literature in the study of the various IR, submillimeter, and radio populations, Blain et al. (1999a, 1999b) have demonstrated that models that are not strongly peaked, in particular those that flatten beyond a certain redshift, have problems overpredicting the submillimeter background. While it is clear that it will not be possible to distinguish minute details of evolutionary form, this study aims to constrain its gross properties.

2.1. *Fitting the Multiwavelength Counts and Backgrounds*

Studies invoking a pure density evolution of the FIR galaxy population have been shown to grossly overpredict the cosmic infrared background and are hence unphysical. Other authors have considered both density and luminosity evolution of the FIR population, successfully recovering both the number counts and backgrounds (Franceschini et al. 2001; Chary & Elbaz 2001; Xu et al. 2003). However, it has been shown that these observational properties can be explained within models adopting only luminosity evolution (Blain et al. 1999a). Given its simplicity (with reduced parameters), we adopt a similar pure luminosity evolution to examine the cosmic history of FIR galaxies.

The evolution is modeled in a simple form: $\Phi(L, C) = \Phi_0(L/g(z), C')$. The color term of our LF (C' rest frame $60/100$ μm flux ratio) does not evolve but rather continues to scale with FIR luminosity as found locally. C03 and Blain et al. (2003) have demonstrated that this lack of significant $60/100$ μm color evolution appears to hold at least out to moderate redshifts ($0.3 < z < 0.9$) in a sample of *IRAS*-detected ULIRGs of Stanford et al. (2000). As the form of the L–T distribution remains fixed for all redshifts, the only remaining parameter is $g(z)$. It should be noted that Dunne et al. (2000) suggested that the *IRAS* galaxy luminosity function may be incomplete, missing cold galaxies. Recently, this conclusion has been strengthened by observations by Klaas et al. (2001) and Bendo et al. (2002, 2003). Given that the current study is tied to *IRAS*, this effect will accentuate the features of cold galaxies presented in this paper, although the degree of *IRAS* underrepresentation of cold galaxies must be quantified to fully explore this.

Adopting a Monte Carlo approach, luminous infrared galaxies are drawn randomly from the evolving distribution function. A galaxy thus selected from this model universe is then assigned a template spectral energy distribution from the catalog of Dale et al. (2001) and Dale & Helou (2002), parameterized by the $60/100$ μm color and normalized to the FIR luminosity. This model scenario does not incorporate the intrinsic scatter in the FIR/radio correlation (0.2 dex), as was done in Chapman et al. (2002; hereafter C02). Rather, this study concentrates on the properties of the intrinsic dust temperature distribution, which locally shows a larger scatter (0.3 dex) than the FIR/radio correlation and should be expected to dominate the high-redshift radio and submillimeter properties.

C02 adopted an evolution function with a simple power-law peak, $g(z) \propto (1+z)^4$ out to a break redshift and dropping thereafter as $g(z) \propto (1+z)^{-4}$, with no discontinuity in the zeroth derivative. This power-law index was chosen and provided reasonable descriptions of submillimeter and radio data, allowing a fit to the submillimeter counts and background (C02). This evolution form coupled with the bivariate model provided a reasonable fit over the submillimeter fluxes represented by our data ($5 < S_{850\mu m} < 15$ mJy). However, the model produced too many bright submillimeter sources, with an increasing excess of >20 mJy sources with increasing peak redshift. This toy model cannot be considered physical, and the culprit for the excess bright sources is found to be in the peak turnover in $g(z)$ producing a spike of luminous sources at the tip of our color-magnitude diagram (CMD) coupled with the range of T_d for each luminosity. While this peak model was useful for illustrating various selection effects (as in C03), it must be replaced with a more realistic evolution form to provide a more accurate description of the submillimeter population, and, therefore, the functional form of Blain et al. (1999b) is adopted: $g(z) = (1+z)^{3/2}\mathrm{sech}^2[b \ln(1+z) - c]\cosh^2 c$.

In constraining the form of the above evolution model, galaxy submillimeter/radio distributions with varying values of b and c were constructed and compared to the differential number count models at 850 μm (Barger et al. 1999) and 15 μm (Elbaz et al. 1999). For a particular set of values of b and c, the number counts are scaled to minimize the residuals between the Monte Carlo simulation and the modeled number counts. For the purposes of this study, it was assumed that the models possessed an uncertainty of 0.2 dex, and the resulting best values of b and c are $2.10^{+0.50}_{-0.60}$ and $1.81^{+0.24}_{-0.46}$, respectively. The range of parameters effectively shift the z_{peak} of the peak evolution function such that $z_{\mathrm{peak}} = 1.8^{+0.9}_{-0.4}$.

Bivariate model counts from our best-fit simulation at 850, 170, 160, 70, 24, and 15 μm are shown in the top panel of Figure 1. The models are overlaid on measured SCUBA (850 μm; Blain et al. 2002) and *ISO* (15 μm, Elbaz et al. 1999; and 170 μm, Dole et al. 2001) counts from the literature. For comparison, we overlay the model counts of Dole et al. (2003) as dashed lines, which agree remarkably well with our models. At the brightest end of the counts, our model is constrained by the length of our Monte Carlo runs, and we are dominated by small-number statistics. The bottom panel of Figure 1 compares the integrated flux in the bivariate model to the observed cosmic infrared background (CIB; Fixsen et al. 1998); again, the best-fit model from the counts accounts for the observed CIB distribution.

Previous modeling (C02) found a reasonable fit to the data with a peak evolution redshift of $z = 3$, when all objects were assumed to have hot dust temperatures ($\sim$50 K), similar to the local ULIRG, Arp 220. The current model ties the dust temperature of a source to its luminosity as observed locally for the *IRAS* 1.2 Jy sample galaxies, whereby a galaxy with a FIR luminosity of 10^{12} $L_\odot$ has $T_d = 35$ K and dust emissivity $\beta = 1.6$, as described in Dale & Helou (2002). In addition, the $60/100$ μm color distribution observed locally is adopted in the FIR luminosity function, resulting in a tail of cold, luminous galaxies, which are preferentially selected with SCUBA at 850 μm (e.g., Blain et al. 1999b; Eales et al. 1999; Chapman et al. 2003a). As expected (see also the discussion in C02), the

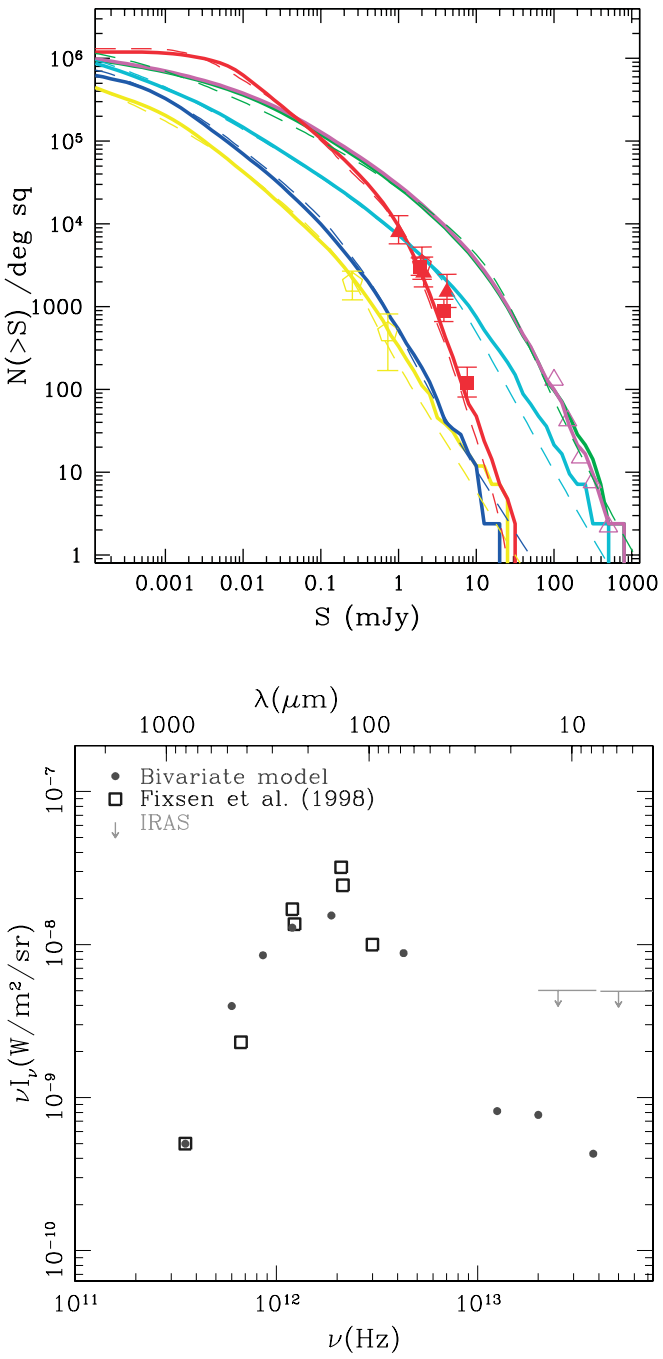


FIG. 1.—*Top*: Bivariate model count from our best-fit simulation at 850 μm (*red*), 170 μm (*purple*), 160 μm (*green*), 70 μm (*cyan*), 24 μm (*blue*), and 15 μm (*yellow*), compared to SCUBA and *ISO* counts from the literature (*points*). For comparison, we overlay the model counts of Lagache et al. (2003) as dashed lines. *Bottom*: Integrated bivariate model compared to the cosmic infrared background of Fixsen et al. (1998). The upper limits at 12 μm and 24 μm are drawn from Scott et al. (2001). [*See the electronic edition of the Journal for a color version of the bottom panel.*]

best-fitting peak evolution redshift must be lower if a population of luminous colder sources exists at high redshifts.

3. PREDICTIONS FOR SPITZER GALAXIES

3.1. *Redshift and Color-Color Distributions*

Taking our best-fit evolution functions for both the bivariate and single-variable models, we predict redshift distributions for galaxy surveys at 24, 70, 160, and 850 μm, covering an area of 1 deg^2. We place flux density thresholds on our simulation, comparable with a shallow *Spitzer* observation such as the First Look Survey.[3] A deep survey is also analyzed, representing flux densities 5 times fainter in all bands (ignoring the effects of confusion in the longer wavelength beams for now). For the submillimeter surveys, the shallow survey is set at the confusion limit of SCUBA (2 mJy). The survey reaching 5 times this depth will be achievable with future instruments such as the Atacama Large Millimeter Array (ALMA).

The comparisons are shown in Figure 2. Because of the spread in temperature at each luminosity, with increasing numbers of hot sources lying at higher redshifts and conversely colder sources at lower redshifts, the effect of the bivariate distribution is to increase the numbers of both high- and low-redshift sources, relative to the single-variable model. In considering photometric redshifts for *Spitzer* sources, or indeed in simply trying to preselect subpopulations of *Spitzer* sources with a given range in redshift or temperature properties, it is, therefore, crucial to have a calibrated estimate of the source distributions in the various color-color planes.

Color-color diagrams of galaxies in a 24 μm flux-limited survey ($S_{24\mu m} > 0.2$ mJy) are shown in Figure 3. The left panel presents the distribution of galaxies assuming the univariate luminosity-temperature relation, whereas the right panel presents the corresponding distribution for the bivariate case. In each panel, objects are color-coded by redshift: $0 < z < 1$ (*cyan*), $1 < z < 2$ (*blue*), $2 < z < 3$ (*green*), and $z > 3$ (*red*). It is apparent that the distribution of galaxies in the two figures is markedly different, with the introduction of a bivariate form of the luminosity function changing the relative density of galaxies in the color-color plane; this behavior is also seen in other color-color planes. Clearly, while different redshift regimes can be delineated in the color-color plane, allowing the determination of photometric redshifts for galaxies, the redistribution of galaxies in the plane due to the introduction of the bivariate distribution implies that such determinations depend on the nature of the luminosity-temperature relationship.

While our model has not yet been tuned to fit the deep, multiwavelength *Spitzer* counts, it already emphasizes that the source distributions as a function of redshift and SED can vary significantly, from the bivariate case to the single-temperature luminosity models. Upcoming papers will explore this issue more fully, once deep *Spitzer* data are available to further constrain our models.

In C03 we presented the baseline assumption in this model: the local $S_{60\mu m}/S_{100\mu m}$ as a function of L holds at all redshifts, simply extrapolating the local L–C relation to the required luminosities. We have now fit this model explicitly to the pre-*Spitzer* submillimeter and mid-infrared counts to constrain the evolution function and used this tuned model to make predictions on the populations observed in the *Spitzer* wavelengths (8, 24, 70, and 160 μm).

In Figure 4, we show the $L_{\rm TIR}$ distribution as a function of redshift. Each pair of panels represents a particular wave band (8, 24, 70, and 160 μm), with the left panel in a pair representing the bivariate model and the right panel presenting the univariate case. Until we apply a flux limit to the figure (*darker points*), there is no difference between the visualizations, since they have the same luminosity evolution formalism.

[3] See http://ssc.spitzer.caltech.edu/fls.

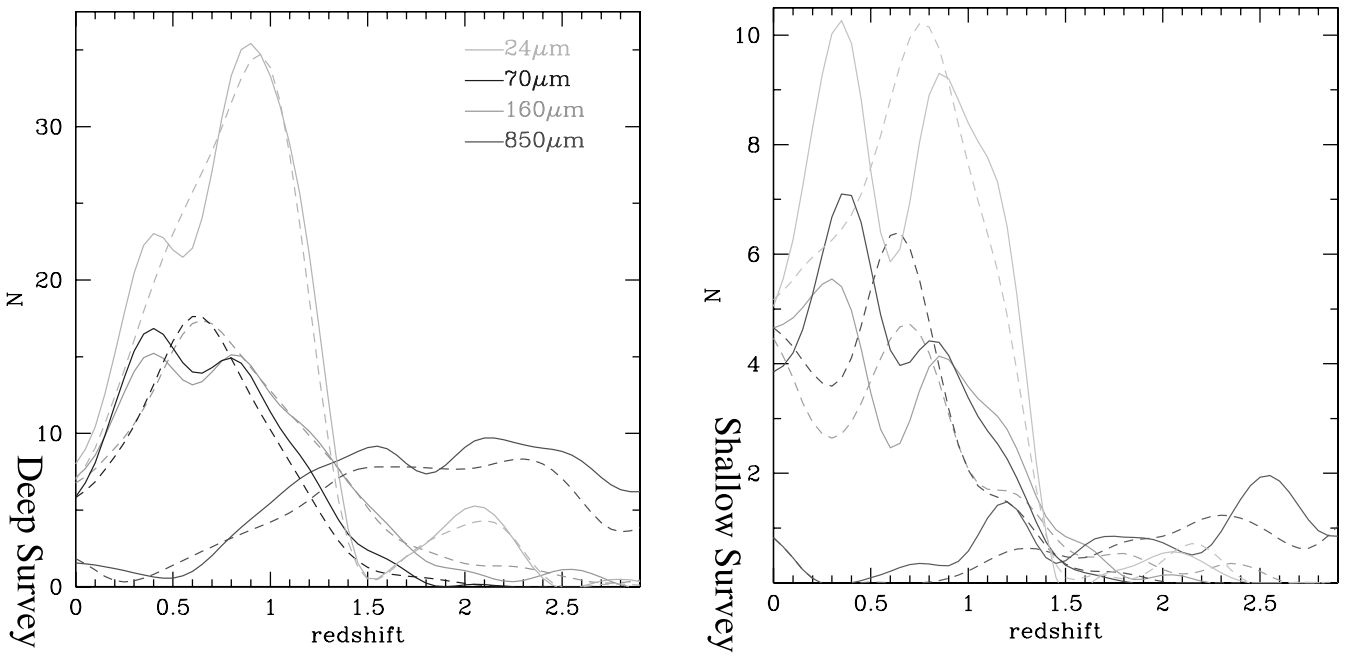


FIG. 2.—Redshift distributions at 24, 70, 160, and 850 μm. The distributions are shown for both a deep (*left*) and a shallow (*right*) survey, in the bivariate (*solid lines*) and single-variable (*dashed lines*) models. The effect of the bivariate distribution is to increase the numbers of both high- and low-redshift sources, relative to the single-variable model, because of the temperature spread. The shallow survey is comparable to the expected First Look Survey (FLS), with the 850 μm survey being typical of current wide-field SCUBA surveys. The deep survey is scaled at all wavelengths by a factor of 5.

Figure 4 is our Monte Carlo representation of the evolving LF; vertical slices reveal the dual power law $\Phi(L, C)$ at each redshift.

When flux-limited surveys are considered in the context of Figure 4, differences in the two models become manifest. In the case of the single-variable distribution, each $L_{\rm TIR}$ point maps uniquely to a flux for a given wavelength. However, in the bivariate LF, each $L_{\rm TIR}$ point corresponds to a probability distribution of fluxes corresponding to the lognormal distribution in $S_{60\mu{\rm m}}/S_{100\mu{\rm m}}$ and the associated range of SED templates that can be tied to the $L_{\rm TIR}$ value. The sensitivity limits in the various bands are shown for the deepest surveys with *Spitzer*. The structure in the 8 and 24 μm surveys is a result of polycyclic aromatic hydrocarbon (PAH) bands (rest $\sim$10 μm) being redshifted through the *Spitzer* 24 μm filter. At 70 and 160 μm, the SED is relatively smooth.

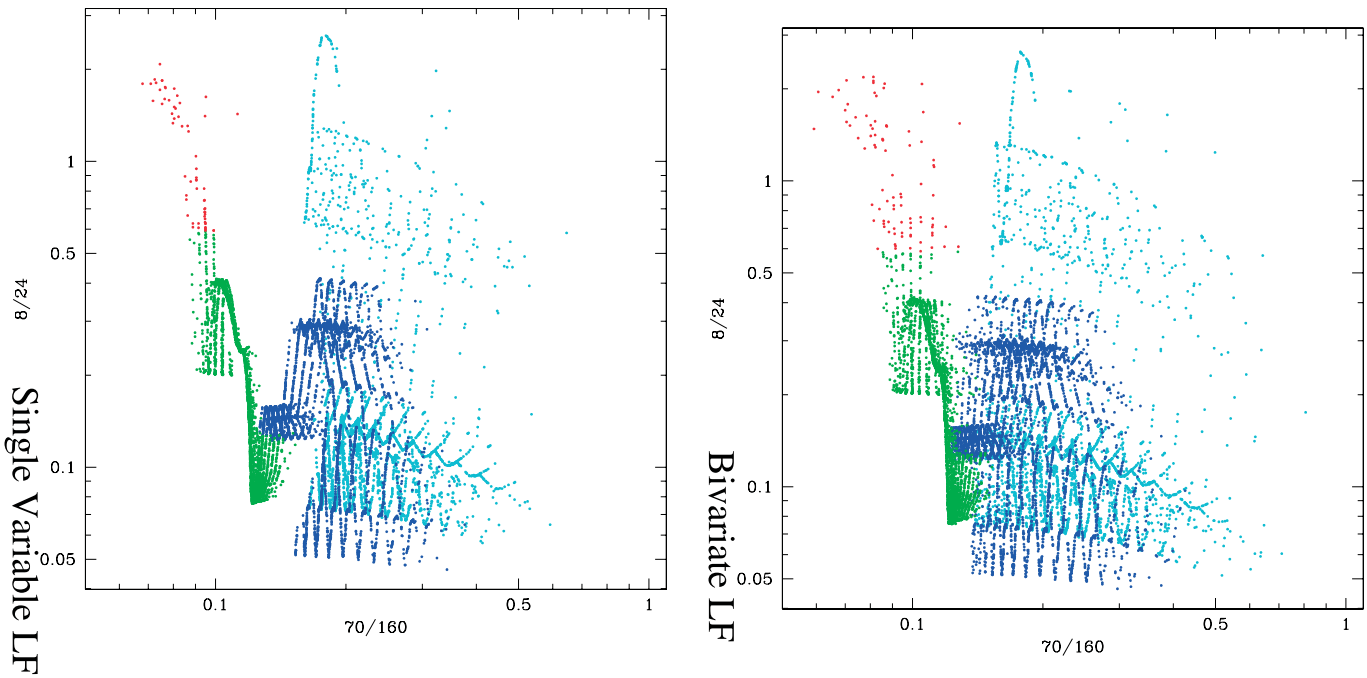


FIG. 3.—Color-color diagrams of galaxies in a 24 μm flux-limited survey ($S_{24\mu{\rm m}} > 0.2$ mJy). The left panel presents 70/160 μm vs. 8/24 μm for the univariate case, whereas the right panel presents the same distribution for the bivariate case. Objects are color-coded by redshift: $0 < z < 1$ (*cyan*), $1 < z < 2$ (*blue*), $2 < z < 3$ (*green*), and $z > 3$ (*red*).

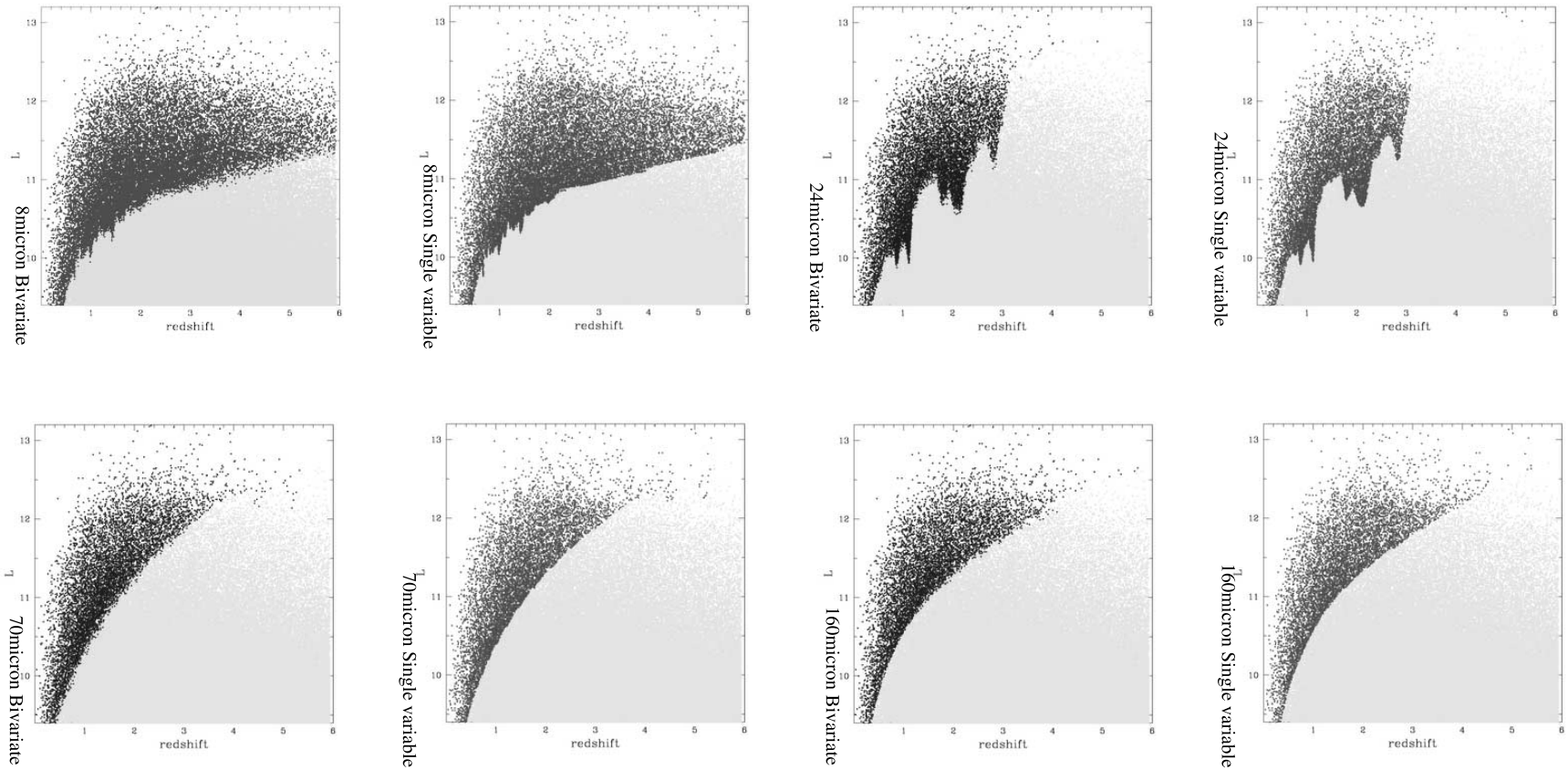


FIG. 4.—Comparison of our Monte Carlo representation of the evolving $\Phi(L, C)$ (*top panels*) to an evolving univariate model LF (*bottom panels*) with a one-to-one mapping of luminosity to color. Each point represents only luminosity, and thus the distributions are equal in both cases. The difference between models is apparent when flux-limited surveys are defined on the model points. We overlay flux-limited samplings of the model points with darker symbols. In the single-variable LF model, luminosities map uniquely to fluxes, and lines can be drawn that reflect fixed temperatures. The top panels are for 8 and 24 μm, while the bottom panels are for 70 and 160 μm.

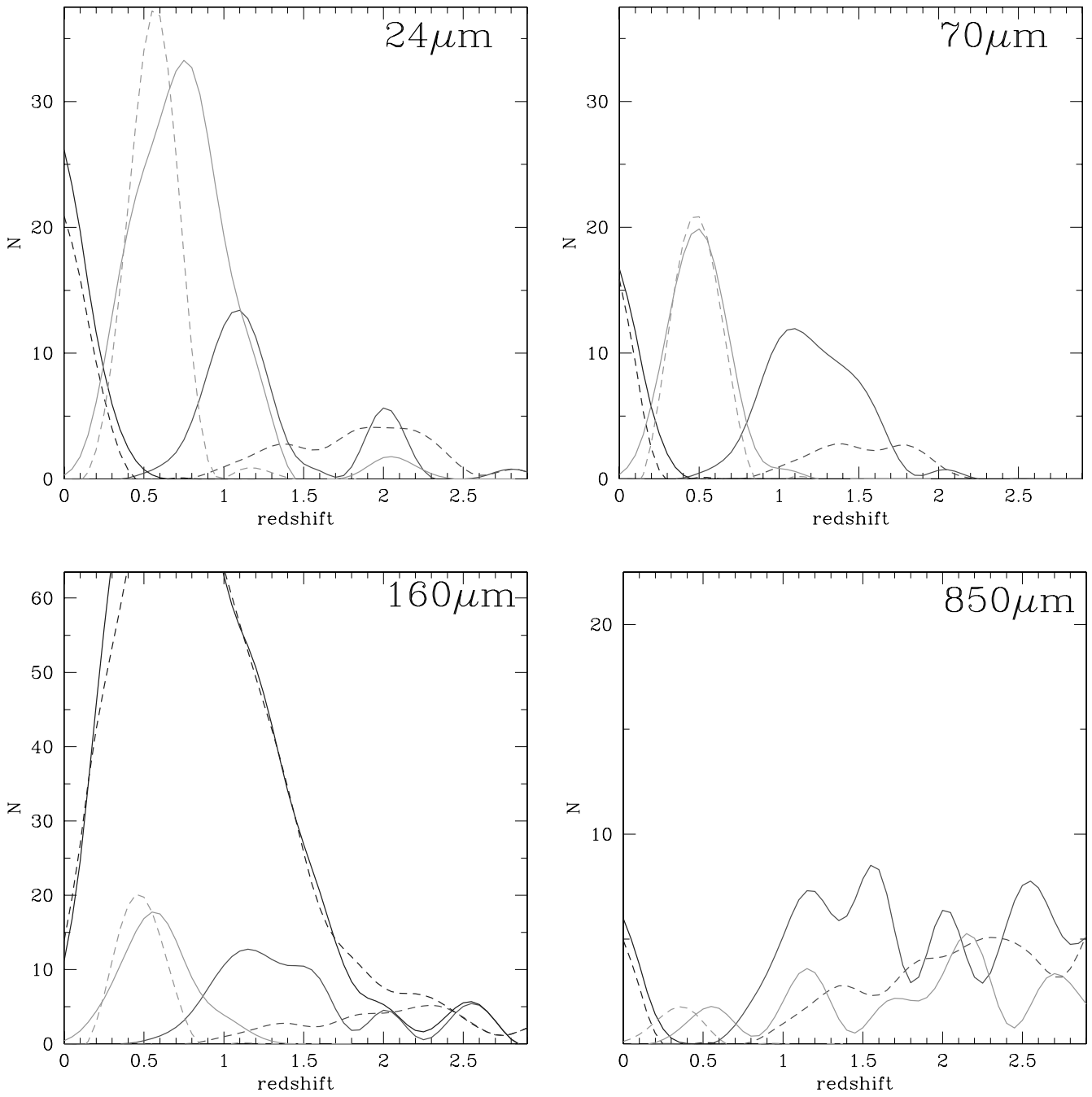


FIG. 5.—Comparison of the dust temperature distributions as a function of redshift for the $\Phi(L, C)$ (*solid lines*) to an evolving model LF with a one-to-one mapping of luminosity to color (*dashed lines*). Distributions are shown for hot (*light gray lines*, $T_d > 40$ K), medium (*medium gray lines*, $28 < T_d < 33$ K), and cold (*black lines*, $T_d < 25$ K). The panels are divided by wavelength, as indicated.

The effect is subtle in Figure 4, as both the luminosity function and the color distribution are scattering the observed fluxes, largely canceling dramatic differences in the effective luminosity limits probed with redshift. However, the most important difference between the bivariate and luminosity-only models is apparent in Figure 4: in the simpler $\Phi(L)$ model, the flux limit for a given wavelength translates at each redshift into a transition range of luminosities, within which galaxies are or are not detected depending on their color. For surveys selecting sources along the hot dust side of the graybody peak, that being the case for all the accessible wavelengths of *Spitzer* except 160 μm, colder luminous sources will be missed, and hotter low-luminosity sources will be preferentially detected.

The detection efficiency at high redshift of *Spitzer* is adversely affected by the steep Wien slope of the far–mid-infrared SED, making more distant sources difficult to detect and resulting in the steep sensitivity curve in Figure 4. The result is that near the sensitivity limit of *Spitzer*, surveys will be dominated by the large numbers of sources lying both above and below any fixed temperature cut. For hotter dust temperatures, an excess of a factor greater than two of sources is predicted by the $\Phi(L, C)$ model. All sources are luminous enough to be detected regardless of their temperature, and there are far more lower luminosity sources that are boosted by hot dust temperatures because of the bivariate LF than vice versa.

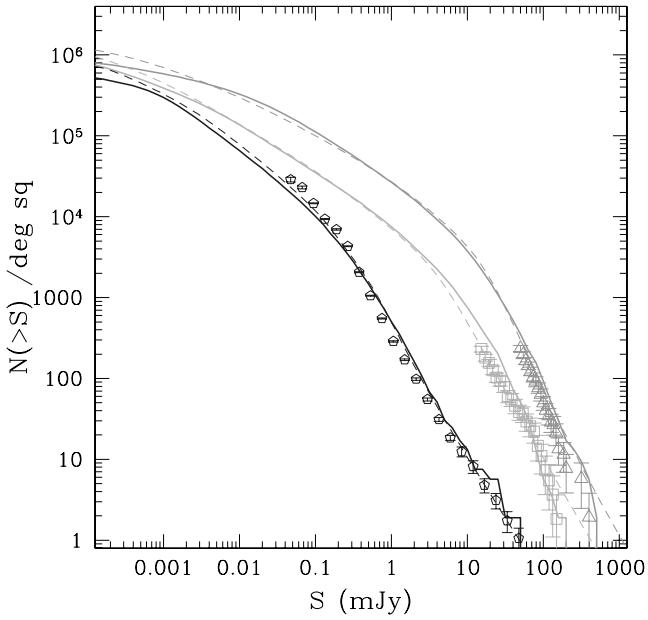


FIG. 6.—Same as top panel of Fig. 1, but now the bivariate model is compared to the recently compiled *Spitzer* counts at 24 μm (*black*), 70 μm (*medium gray*), and 160 μm (*dark gray*) (Dole et al. 2004; Papovich et al. 2004).

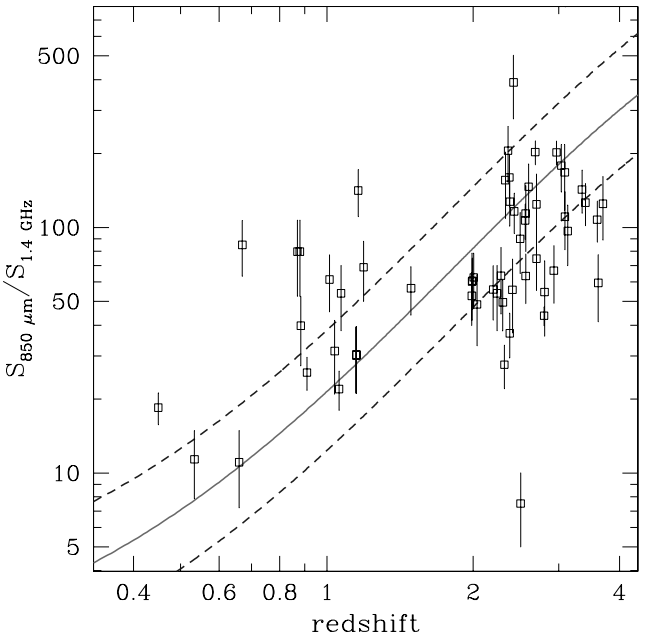


FIG. 7.—$S_{850\mu m}/S_{1.4GHz}$ indices for SMGs with redshifts, compared to our model prediction, with the dashed lines corresponding to 1 σ scatter in the population of model galaxies. Note that the model includes only the range of dust temperatures observed locally in the *IRAS* population, whereas a variation in the radio-to-FIR ratio likely increases the scatter further.

Figure 5 demonstrates these model differences explicitly, demonstrating that many more sources are detected in the extremes of the temperature distributions in the $\Phi(L, C)$ model. Moreover, the predicted distributions are often radically different in form in the $\Phi(L, C)$ case. The double-peaked profile apparent in the redshift distributions presented in Figure 2 is a result of temperature differences in the underlying IR population. Figure 5, therefore, illustrates the strongest differences between the univariate and bivariate models.

Recently, deep counts at 24, 70, and 160 μm, obtained with the Multiband Imaging Photometer on *Spitzer* (MIPS), have become available (e.g., Dole et al. 2004; Papovich et al. 2004). This presents further opportunities to test the efficacy of the bivariate model. Figure 6 presents the bivariate model prediction for the *Spitzer* MIPS bands with the observed counts overlaid. Generally, the observed trends are reproduced, but discrepancies are apparent, most notably a deficit in the *Spitzer* counts between 1 and 10 mJy. Addressing these discrepancies is beyond the scope of this present work and will be reserved for further study.

4. STUDYING THE SUBMILLIMETER GALAXIES

Spitzer data are beginning to be analyzed in depth, with spectroscopic follow-up just getting under way. Detailed comparison of our models with the *Spitzer* sources will be the focus of an upcoming paper, once an initial census of the *Spitzer* surveys are complete. However, our understanding of the deepest 850 μm submillimeter sources has recently reached a relatively mature state, with the measurement of spectroscopic redshifts for a large sample (Chapman et al. 2003c; S. Chapman et al., in preparation). In this section, we compare our predictions for the submillimeter galaxies (SMGs) directly with the measurements.

The $S_{850\mu m}/S_{1.4GHz}$ ratio provides a measure of the degenerate quantity $(1 + z)/T_d$ (Blain et al. 1999b), coupled with any evolution in the FIR/radio correlation. As the redshift parameter has now been independently measured for the SMGs, we can directly compare the $S_{850\mu m}/S_{1.4GHz}$ predictions of our model to the SMGs. Figure 7 shows the $S_{850\mu m}/S_{1.4GHz}$ indices for SMGs with redshifts, compared to our model prediction. Note that the model includes only the range of dust temperatures observed locally in the *IRAS* population, whereas a variation in the radio-to-FIR ratio likely increases the scatter further.

The actual submillimeter population appears to span a larger range than the local *IRAS* galaxy population, although there are some caveats to consider. The SMG surveys are missing cold sources in the radio detection criterion, and thus there is some asymmetry in the actual observations toward hotter dust temperatures. At low redshifts, there are some apparently very cold galaxies that are not predicted by the local *IRAS* extrapolation. If SMG identifications are correct, they may signal a sparse population whose closest local analogs would be the radio-deficient galaxies that Roussel et al. (2003) interpret as nascent starbursts. These radio-deficient objects are relatively rare, at about 1% of the local population, since they would have to be found during the first few million years of the starburst phase.

A remaining question is the interpretation of sources in our model. Ongoing debates discuss whether accretion power from supermassive black holes or bursts of star formation is heating the dust in ULIRGs. Our model has not assumed either explicitly. Rather, we have taken the distribution of 60/100 μm color found locally in the *IRAS* galaxy population and assumed that it describes galaxies at all redshifts. However, AGNs are typically known to have warmer colors, and our model may not accurately reflect their possibly larger contributions at higher redshift and luminosity.

A test for AGN contribution is whether the SMGs are unusually bright in the X-ray range, in which even obscured AGNs should reveal themselves, penetrating high columns of gas. The radio identification of the submillimeter sources has allowed their locations to be pinpointed. In Barger et al. (2001a, 2001b), it was pointed out that approximately 10% of the X-ray sources were

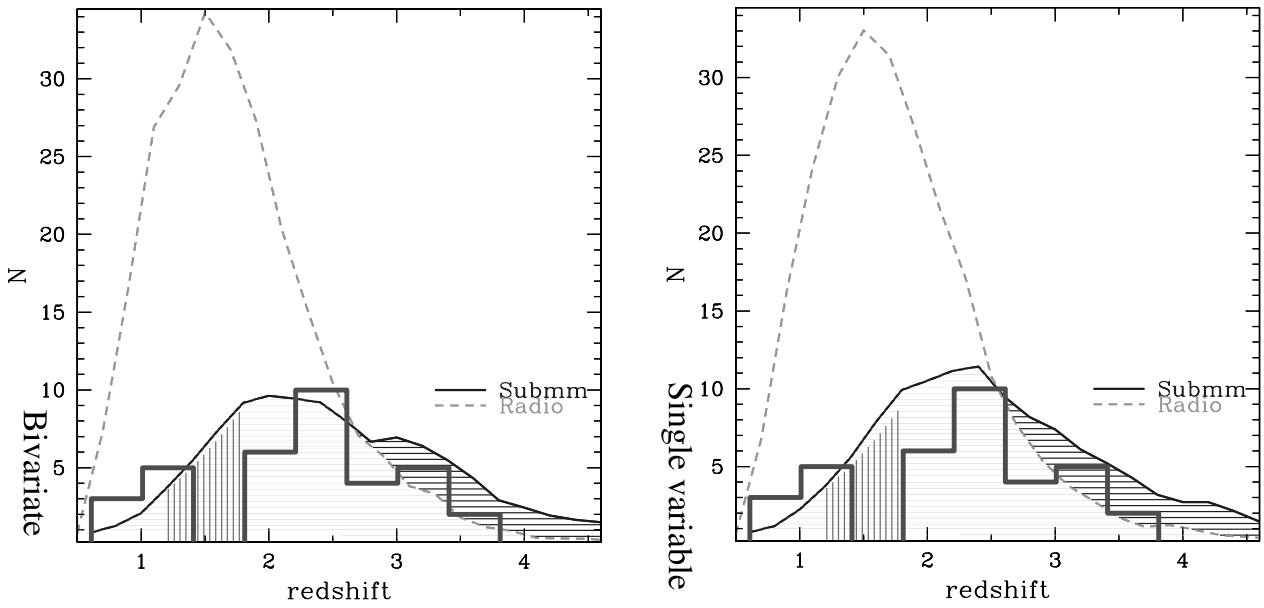


FIG. 8.—Predicted redshift distributions for radio (*dashed lines*) and submillimeter (*solid lines*) wavelengths. The left panel shows the prediction for the bivariate model, while the right panel shows the single-variable LF model. Mild differences in the predicted $N(z)$ are observed between models, which the data cannot differentiate between. The dark shaded region in both panels reveals the submillimeter sources that are not expected to be detectable in the radio. The light shading shows the *spectroscopic desert*, in which no strong emission lines are shifted into the optical atmospheric window. Overlaid as a histogram is the measured redshift distribution for radio-detected submillimeter galaxies from Chapman et al. (2003a).

submillimeter detected in the *Chandra* megasecond exposure centered on the HDF. The 2 Ms exposure in this field has detected the majority ($\sim$90%) of the radio SMGs (Alexander et al. 2003). As this radio-identified submillimeter population represents $\sim$65% of the total blank-field SCUBA population at $S_{850\mu m} > 5$ mJy, this implies that a fraction >60% of the total SCUBA population is detectable in a 2 Ms *Chandra* exposure. The typical inferred star formation rate from this analysis is roughly 1000 $M_{\odot}$ yr^{-1}, similar to that deduced from the submillimeter luminosities.

The sources with considerably higher X-ray luminosities, in which the X-ray implied star formation rate would severely exceed the submillimeter estimate, suggest that an AGN must be generating the X-ray emission, and we emphasize that our model does not account for such sources explicitly. Note, however, that in Figure 7, only one source explicitly stands out from the distribution because of radio excess over the model expectations.

Let us now look specifically at the differences between the bivariate and single-variable models. The counts and redshift distributions are natural measurable outputs from our model. The univariate model predicts a one-to-one mapping of $S_{850\mu m}/S_{1.4GHz}$ with redshift (for a fixed Q-value; Helou et al. 1985); clearly the observed scatter seen in Figure 7 cannot be explained by such a simple mapping. The bivariate model naturally introduces a scatter into this relationship, and the dashed lines in Figure 7 correspond to the 1 σ width of the $S_{850\mu m}/S_{1.4GHz}$ distribution as a function of redshift. It is a straw-man argument to compare a single SED model to our data, which provides an unphysically narrow range of submillimeter/radio colors (e.g., C02). A more realistic approach is to constrain the width of the color distribution of our best-fitting bivariate model until there is only a single temperature SED associated with a given luminosity. This single-variable model can be thought of as mapping the dust temperature monotonically to the source luminosity.

We first extract the counts from our models and compare directly with the measured field counts. Both models are able to fit the counts well within current measurement errors. The submillimeter counts are insensitive to the width in color, C', in our model because of the degeneracy in T_d versus redshift. Therefore, neither of these models is better constrained by the submillimeter counts. The FIR background (Puget et al. 1996; Fixsen et al. 1998) also provides little constraint on the detailed form of the high-z evolution, requiring only that the evolution function fall off quickly enough at high redshifts to avoid generating too high an energy density. Both models generate submillimeter and FIR background values midway between the measurements of Puget and Fixsen. The model is therefore self-consistent as a generalization to the evolution of the entire submillimeter population. While the model does not provide a unique description of the submillimeter galaxies, it is physically motivated by the detailed properties of local and moderate redshift *IRAS* galaxies.

We can use our model to predict the redshift distributions for radio (1.4 GHz) and submillimeter (850 μm) galaxies. In Figure 8, we show the prediction for the bivariate model (*left panel*) compared to the single-variable LF model (*right panel*). The bivariate scenario marks a difference in the predicted $N(z)$, in which a deficit of sources at the redshift peak are seen relative to the single-variable model, with a corresponding boost to the higher redshift sources. This behavior was described in C02, in which the FIR/radio distribution provides a similar effect. The shaded regions between the radio and submillimeter model curves reveal the submillimeter sources that are not expected to be detectable in the radio. In the bivariate model, a range of hotter dust temperatures for a given luminosity leads to a higher redshift range for radio detectability. While not statistically significant, the bivariate model appears to follow the observed redshift distribution.

Understanding of the full redshift distribution for the submillimeter population through deep optical and millimeter spectroscopy will provide a strong test of these models and the applicability of the local bivariate L–T relation to this high-redshift population. The discovery of the redshift distribution

for the radio-detected submillimeter galaxies (Chapman et al. 2003a, 2003b) is shown overlaid on our models in Figure 8. A remarkable agreement is found between the data and our model, with a preference for the flattened distribution and expanded range of redshifts in the bivariate picture. We conclude that submillimeter galaxies exhibit at least as large a range in dust temperatures as local *IRAS* galaxies and likely a larger range.

The anonymous referee is thanked for their constructive comments. We gratefully acknowledge the extensive help of K. Witherington with the Canada-France-Hawaii Telescope 12k camera archives and J. C. Cuillandre for the creation and support of the FLIPS data reduction pipeline. G. F. L. thanks the Australian Nuclear Science and Technology Organization (ANSTO) for financial support.

REFERENCES

Alexander, D., et al. 2003, AJ, 126, 539
Barger, A. J., Cowie, L. L., Bautz, M. W., Brandt, W. N., Garmire, G. P., Hornschemeier, A. E., Ivison, R. J., & Owen, F. N. 2001a, AJ, 122, 2177
Barger, A. J., Cowie, L. L., & Sanders, D. B. 1999, ApJ, 518, L5
Barger, A. J., Cowie, L. L., Steffen, A. T., Hornschemeier, A. E., Brandt, W. N., & Garmire, G. P. 2001b, ApJ, 560, L23
Bendo, G. J., et al. 2002, AJ, 124, 1380
———. 2003, AJ, 125, 2361
Blain, A., Barnard, V., & Chapman, S. C. 2003, MNRAS, 338, 733
Blain, A., et al. 1999a, MNRAS, 302, 632
———. 1999b, MNRAS, 309, 715
Blain, A. W., Smail, I., Ivison, R. J., Kneib, J.-P., & Frayer, D. T. 2002, Phys. Rep., 369, 111
Chapman, S. C., Blain, A., Ivison, R., & Smail, I. 2003a, Nature, 422, 695
Chapman, S. C., Helou, G., Lewis, G. F., & Dale, D. 2003b, ApJ, 588, 186 (C03)
Chapman, S. C., Lewis, G., Scott, D., Borys, C., & Richards, E. 2002, ApJ, 570, 557 (C02)
Chapman, S. C., et al. 2003c, ApJ, 585, 57
Chary, R., & Elbaz, D. 2001, ApJ, 556, 562
Condon, J. 1992, ARA&A, 30, 575
Dale, D., & Helou, G. 2002, ApJ, 576, 159
Dale, D., et al. 2001, ApJ, 549, 215
Dole, H., Lagache, G., & Puget, J.-L. 2003, ApJ, 585, 617
Dole, H., et al. 2001, A&A, 372, 364
———. 2004, ApJS, 154, 87
Dunne, L., et al. 2000, MNRAS, 315, 115
Eales, S., et al. 1999, ApJ, 515, 518
Elbaz, D., et al. 1999, A&A, 351, L37
Fisher, K., et al. 1995, ApJS, 100, 69
Fixsen, D. J., Dwek, E., Mather, J. C., Bennett, C. L., & Shafer, R. A. 1998, ApJ, 508, 123
Franceschini, A., Martin, C., & Schiminovich, D. 2001, A&A, 378, 1
Helou, G., et al. 1985, ApJ, 298, 7
Ivison, R., et al. 2002, MNRAS, 337, 1
Klaas, U., et al. 2001, A&A, 379, 823
Lagache, G., Dole, H., & Puget, J.-L. 2003, MNRAS, 338, 555
Papovich, C., et al. 2004, ApJS, 154, 70
Puget, J.-L., Abergel, A., Bernard, J.-P., Boulanger, F., Burton, W. B., Desert, F.-X., & Hartmann, D. 1996, A&A, 308, L5
Roussel, H., Helou, G., Beck, R., Condon, J.-J., Bosma, A., Matthews, K., & Jarrett, T.-H. 2003, ApJ, 593, 733
Scott, D., Borys, C., Halpern, M., Sajina, A., Chapman, S., & Fahlman, G. 2001, in Deep Millimeter Surveys: Implications for Galaxy Formation and Evolution, ed. J. D. Lowenthal & D. H. Hughes (River Edge: World Scientific), 160
Smail, I., Ivison, R. J., & Blain, A. W. 1997, ApJ, 490, L5
Soifer, B. T., & Neugebauer, G. 1991, AJ, 101, 354
Stanford, S. A., Stern, D., van Breugel, W., & De Breuck, C. 2000, ApJS, 131, 185
Xu, C. K., Lonsdale, C., Shupe, D., Franceschini, A., Martin, C., & Schiminovich, D. 2003, ApJ, 587, 90